ARTICLES

Monte Carlo Simulations of Polyelectrolyte−Protein Complexation

Fredrik Carlsson,*,† Per Linse,‡ and Martin Malmsten†,§

Institute for Surface Chemistry, Box 5607, SE-114 86 Stockholm, Sweden, Physical Chemistry 1, Center for Chemistry and Chemical Engineering, Lund University, Box 124, SE-221 00 Lund, Sweden, and Department of Chemistry, Surface Chemistry, Royal Institute of Technology, SE-114 44 Stockholm, Sweden

Received: January 29, 2001; In Final Form: April 11, 2001

The complexation between one polyelectrolyte and one protein has been examined by employing a simple model system solved by Monte Carlo simulations. The polyelectrolyte was composed of a sequence of negatively charged hard spheres, and the protein was represented by a hard sphere with embedded pH-dependent discrete charges, the positions of which were taken from lysozyme. A short-range attractive interaction between the polyelectrolyte and the protein accounting for hydrophobic interactions completed the model. The complexation was found to depend decisively on the charge status of the protein model as well as on the presence of the short-range attractive interaction. In particular, the complexation weakens at decreasing ionic strength except for the highest positive protein net charge considered, and in the absence of the short-range attraction, a positively charged protein was required to obtain a complex. The distribution of the polyelectrolyte beads was inhomogeneous at the protein surface, and the polyelectrolyte contracted upon complexation. Finally, the protein model with discrete charges gave a stronger complex than the corresponding protein model with a homogeneous surface charge density.

Introduction

Protein−polymer complexes are of great importance in a variety of contexts within protein purification, drug delivery, food technology, and biotechnology. Experimentally, the complexation has been studied extensively, and also, several review articles have been published.[1−6] A number of features have been found to be of importance for the complexation, including the protein−polymer interaction and the polymer molecular weight, as well as the nature of the protein. Due to the charged nature of proteins, electrostatic interactions play a particularly important role, and so-called complex coacervation between oppositely charged proteins and (bio)polymers have been studied over almost a century.[7−9] During the past few years, electrostatically driven association between proteins and polymers have been investigated in some detail, e.g., regarding the onset of the complex formation and phase separation,[10−12] the characteristics of the aggregates formed in terms of size and composition, and the effect on these parameters by varying the protein−polymer electrostatic interaction through changing pH. Investigations of the retention of proteins to chromatography columns also deal with the charge asymmetry of proteins and their interaction with polymer beads.[13]

Despite the large practical importance of polymer−protein complexation and the large number of experimental studies on this, there have been relatively few investigations focusing on theoretical models of polymers and surfaces[14−17] or the numerical simulations[18−20] of these effects. This is particularly true for investigations in which the lateral electrostatic heterogeneity of the surface is taken into account. Although the importance of the discrete nature of the electrostatic charges of proteins could be expected to be minor at very low excess electrolyte concentrations where screening effects are minor, this could still be significant at higher ionic strengths. Given this, we report here results from a Monte Carlo study of protein−polymer complexation, in which the discrete nature of the protein charges is taken into account.

In this investigation, the complex between a single protein and a single polyelectrolyte chain in aqueous solution is investigated by Metropolis Monte Carlo simulations. The model employed include excluded volume effects and electrostatic and hydrophobic interactions both for the protein and for the polymer, and the model is expected to capture essential features of the system in a qualitative manner without introducing unnecessary complexity. The protein model was chosen to resemble lysozyme due to (i) the knowledge of the structure of lysozyme, (ii) its nearly spherical shape, (iii) its structural stability, and (iv) its use in experimental investigation on protein−polymer complexation. Thus, we would expect relatively small structural changes in the protein when complexing with polymers.. Different ionic strengths and protein charges corresponding to different pH values are investigated, and the protein−polymer complex is characterized by employing running coordination numbers, the probability of contact between

* Corresponding author. email: fredrik.carlsson@surfchem.kth.se
† Institute for Surface Chemistry.
‡ Lund University.
§ Royal Institute of Technology.

10.1021/jp010360o CCC: $20.00
Published on Web 08/24/2001

the protein and polyelectrolyte beads, and the distribution of polyelectrolyte beads in a plane through the protein center.

Model

The complexation between the protein and the polyelectrolyte at various ionic strengths is modeled using a simple model. The protein and polyelectrolyte are represented by charged hard spheres interacting by (i) electrostatic forces screened by the solvent and the simple electrolyte and (ii) short-range attractive forces.

Polyelectrolyte. The polyelectrolyte is modeled as a chain of $N_{bead} = 60$ charged hard spheres (beads) joined by harmonic bonds with its intrinsic flexibility regulated by harmonic angular energy terms. The chain beads have a radius $R_{bead} = 2$ Å and one elementary charge $Z_{bead} = -1$. The bond and angular energy terms applicable only to the polyelectrolyte are given by

$$U_{bond} = \sum_{i=1}^{N_{bead}-1} \frac{1}{2} k_{bond}(r_{i,i+1} - r_0)^2 \quad (1)$$

and

$$U_{ang} = \sum_{i=2}^{N_{bead}-1} \frac{1}{2} k_{ang}(\alpha_i - \alpha_0)^2 \quad (2)$$

respectively. In eq 1, $r_{i,i+1}$ denotes the separation between beads i and $i + 1$, r_0 the equilibrium separation of the harmonic bond potential, and k_{bond} the bond force constant, whereas in eq 2, α_i denotes the angle formed by $\mathbf{r}_{i+1} - \mathbf{r}_i$ and $\mathbf{r}_{i-1} - \mathbf{r}_i$, α_0 the equilibrium angle of the harmonic angular potential, and k_{ang} the angular force constant. Here, $r_0 = 4.7$ Å, $k_{bond} = 2.4$ kJ/mol/Å^2, $\alpha_0 = 180°$, and $k_{ang} = 0.0048$ kJ/mol/(°)^2 have been used, giving a bare persistence length (the persistence length without electrostatic interaction) of ca. 35 Å.

Protein. The protein is described as a hard sphere with embedded charges representing charges of ionized amino acids. Such a model describes the main features of rigid proteins with a high degree of structural stability, such as lysozyme. The model is kept as simple as possible with no internal degrees of freedom for lysozyme.

Our model of lysozyme was constructed as follows. Atomic coordinates from an X-ray diffraction study of crystalline hen egg white lysozyme were taken from the Brookhaven Protein Data Bank, entry 2LZT.[21] The 32 residues that may carry a net charge were collected, and they and their pK_a values are given in Table 1. The coordinates $\mathbf{r}_i^{PDB}$ of the $N_{atoms} = 32$ (possible) charged atoms of these residues were also collected. In the case where a charge is distributed between several atoms, e. g., between NH1 and NH2 in arginine, one of the atoms were selected. The positions of these atoms were then expressed in a new coordinate system (the coordinate system of the protein) with the origin at $\mathbf{a}_0$ according to $\mathbf{r}_i = \mathbf{r}_i^{PDB} - \mathbf{a}_0$, where $\mathbf{a}_0$ was determined by minimizing $\sum_{i=1}^{N_{atoms}}(\mathbf{r}_i^{PDB} - \mathbf{a}_0)^2$, giving $\mathbf{a}_0 = (-1.4, 15.3, 22.8)$ Å. Thereafter, the atoms were moved radially by Δr_i, making their radial distance identical, i.e., $|\mathbf{r}_i - \Delta\mathbf{r}_i| = r_{atoms}$. The magnitudes of the radial movements Δr_i were chosen so that the numbers of inward and outward moves were equal, resulting in $r_{atoms} = 16.54$ Å. Finally, a hard-sphere radius $R_{prot} = r_{atoms} + 2$ Å $= 18.54$ Å was introduced to give the volume of the protein and to give realistic charge−charge interactions. The radius R_{prot} of our idealized spherical model of lysozyme compares reasonably well with the measured ellipsoidal axes of (22.5, 15, 15) Å [22] and experimentally obtained Stokes radius of 21.3 ± 2 Å.[23]

Finally, due to the fact that (i) some of the positions of the charged atoms in the PDB entry are very close in space, e.g., OD2 of ASP 66 and OH of TYR 53 are only 2.53 Å apart, and (ii) the projection brings them slightly closer, unrealistically short atom−atom distances were obtained. This was remedied by moving these atoms apart at fixed $r_{atoms} = 16.54$ Å, making the smallest distance between all atoms at least 4 Å. Further details are given in Table 2. In Figure 1, the positions of the charged groups before and after the projection and final adjustment are compared.

Simulations were performed with different protein charge distribution corresponding to solutions of different pH. This was achieved by allowing the different atoms to attain $Z_i = 0$, -1, or 1 elementary charges. Here, we considered −COOH and $-NH_3^+$ fully protonized at pH < pK_a and completely depro-

TABLE 1: Titrating Amino Acid Residues, Identity of Charged Atom, and Corresponding pK_a Value in Lysozyme

residue	atom[a]	pK_a[b]
ASP 66	OD2	1.6
ASP 18	OD1	2.0
ASP 87	OD2	2.1
ASP 119	OD2	2.5
GLU 7	OE1	2.6
LEU 129, C−Term.	OXT	3.1
ASP 52	OD2	3.4
ASP 48	OD1	4.3
ASP 101	OD2	4.5
HIS 15	NE2	5.8
GLU 35	OE1	6.1
LYS 1, N−Term.	N	7.9
TYR 23	OH	9.8
TYR 20	OH	10.3
LYS 97	NZ	10.3
LYS 116	NZ	10.4
LYS 13	NZ	10.5
LYS 33	NZ	10.6
LYS 1	NZ	10.8
LYS 96	NZ	10.8
TYR 53	OH	12.1
ARG 5	NH1	12.8
ARG 14	NH2	12.8
ARG 21	NH2	12.8
ARG 45	NH2	12.8
ARG 61	NH2	12.8
ARG 68	NH2	12.8
ARG 73	NH1	12.8
ARG 112	NH1	12.8
ARG 114	NH1	12.8
ARG 125	NH2	12.8
ARG 128	NH2	12.8

[a] PDB nomenclature. [b] From an experimental study[28] at 25 °C and ionic strength $I = 0.1$ M. The pK_a values of the arginine residues were all assigned 12.8, since experimental values were lacking. At increasing pH, these residues were assumed to titrate in raising residue order.

TABLE 2: Final Adjustment of Charged Atoms of the Lysozyme Protein Model[a]

residue	atom[b]	coordinate adjusted	adjustment
LYS 13	NZ	θ	−3.8°
ARG 61	NH2	θ	−4.1°
ARG 68	NH2	φ	+12.4°
ASP 66	OD2	φ	−12.0°
ASP 119	OD2	θ	−2.2°

[a] Separation between atoms smaller than 4 Å was increased to a distance larger than 4 Å by moving one of the atoms using a spherical coordinate system given by (r,θ,φ). [b] PDB nomenclature.

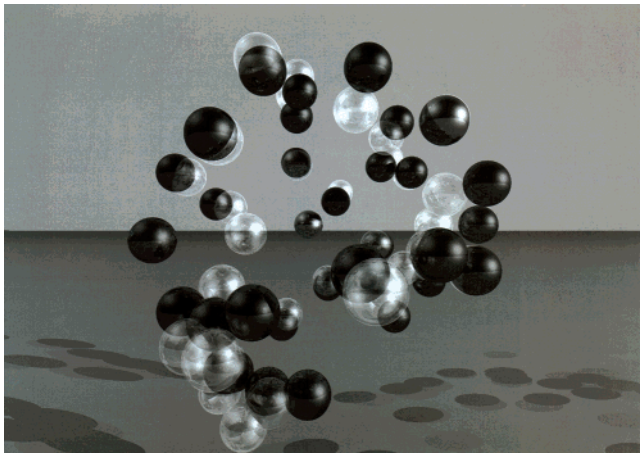

Figure 1. Positions of charged atoms before (transparent spheres) and after (black spheres) the projection and final adjustment (see text for details).

tonated at pH > pK_a. Thus, in the model the protein net charge can be varied from $Z_{prot} = +19$ at very low pH to $Z_{prot} = -13$ at very high pH.

Potential Energy. All interactions between the particles are taken as pairwise additive. With the model described above, the total potential energy of the system becomes

$$U = U_{nonbond} + U_{bond} + U_{ang} \tag{3}$$

where bond and angular terms were given by eqs 1 and 2, respectively. The nonbonded energy is given by

$$U_{nonbond} = U_{hs} + U_{el} + U_{short}$$
$$= \sum_{i<j} u_{ij}^{hs}(r_{ij}) + \sum_{i<j} \frac{Z_i Z_j e^2}{4\pi\epsilon_0\epsilon_r} \frac{1}{r_{ij}} \exp(-\kappa r_{ij}) - \sum_{i<j} \frac{\epsilon}{r_{ij}^6} \tag{4}$$

with

$$u_{ij}^{hs}(r_{ij}) = \begin{cases} 0, & r_{ij} \geq R_i + R_j \\ \infty & r_{ij} < R_i + R_j \end{cases} \tag{5}$$

where r_{ij} is the center-to-center distance between particles i and j, ϵ_0 the permittivity in vacuum, ϵ_r the relative dielectric permittivity of the solvent, $\kappa^{1/2}$ the inverse Debye screening length, and ϵ (>0) a parameter controlling the short-range nonelectrostatic attractive interaction. In the hard-sphere term, the summation extends over the protein center and chain beads; in the electrostatic term, over the protein charges and chain charges; and in the last term, over protein center to chain bead pairs. In eq 4, the Debye−Hückel screening length is given by $\kappa^{-1} = [(1/\epsilon_0\epsilon_r kT)\sum_m (Z_m e)^2 c_m]^{1/2}$, where c_m is the bulk concentration of salt species m. Below, the salt content will be referred by its ionic strength I. Throughout, $T = 298$ K and $\epsilon_r = 78.4$ have been used. At these conditions, $I = 0.1$ M corresponds to $\kappa^{-1} = 9.6$ Å.

In the case of sparsely soluble proteins and polymers, the hydrophobic attraction between them is considerable. Since it is intractable, and also not necessary for our purpose, to treat this attraction in a more refined way, the hydrophobic attraction is here described in a rather crude way by the third term in eq 4. For simplicity, the value of ϵ was assumed to be independent of pH and ionic strength. By performing simulations with different protein charge distributions, corresponding to different experimental pHs at a given ionic strength, the value of ϵ was adjusted to give an onset of the protein−polyelectrolyte complexation at a given pH at that ionic strength according to experimental data. The selected value $\epsilon = 2.6 \times 10^8$ kJ/mol leads to an onset of a complex formation at a protein net charge $Z_{prot} \approx -6$ at the ionic strength 0.1 M. This should be compared with reported lysozyme net charge at the onset of complex formation of $Z_{prot} = -7$, -2.6, -2.6, and -1.6 for the four anionic polymers PVS (sodium poly(vinyl sulfate)), PAMPS (sodium poly(2-acrylamidomethylpropyl sulfate)), PSS (sodium poly(styrenesulfonate)), and NVP-AMPS (copolymer of N-vinylpyrrolidone 50 mol % and 2-acrylamidomethylpropyl sulfate 50 mol %), respectively, at an ionic strength 0.1 M as inferred from quasielastic light scattering measurements.[10,11] These experiments clearly show that complexation may occur even though the protein and the polymer have the same sign of the net charge.

The nonspherical protein charge distribution can be expanded in a series of multipole moments. Comparison will be made between results from simulations (i) with the explicit protein charge model and (ii) with a model where only the leading zero moment (the net charge) of the protein was retained and positioned at the center of the protein. Moreover, in this comparison the prefactor $\exp[\kappa(R_i + R_j)]/[(1 + \kappa R_i)(1 + \kappa R_j)]$, often appearing in the second term of eq 4, is included. The factor is normally attributed to the absence of screening inside a hard sphere and becomes important when $\kappa(R_i + R_j) \gg 1$. Thus, simulations were performed with this factor included using (i) $R_{atom} = 2$ Å and $R_{bead} = 2$ Å in the explicit protein charge model and (ii) $R_{prot} = 18.54$ Å and $R_{bead} = 2$ Å in the more simplified one. Of course, in the former model, the prefactor has a weaker theoretical foundation due to the nonspherical exclusion of the solvent around the protein charges, but it was nevertheless employed in this comparison.

Systems. Simulations were performed for 39 systems obtained by all combinations of ionic strengths $I = 0.05$, 0.1, and 0.5 M and the protein net charges $Z_{prot} = +19$, $+13$, $+10$, $+6$, $+3$, 0, -1, -2, -3, -4, -6, -10, and -13. In addition, systems containing only the polyelectrolyte at the same ionic strengths were also considered to obtain information about the polyelectrolyte properties in the absence of the protein. Moreover, systems containing both protein and polyelectrolyte, but without the attractive $1/r^6$ potential were simulated for some charge and ionic strength combinations for examination of the role of the electrostatic interaction only. Also a system with an uncharged protein and uncharged polymer interacting only with the attractive $1/r^6$ potential, corresponding to the infinite ionic strength, was considered. Finally, simulations with the additional potential prefactor included for a system with the explicit charge model and with the zero moment only, at a protein net charge $Z_{prot} = +10$ and I = 0.1 M, were performed.

Method

Simulation. The model system was solved by Metropolis Monte Carlo (MC) simulations in the canonical ensemble, i.e., at constant number of particles, constant volume, and constant temperature. The particles were enclosed in a cubic box with a box length $L = 400$ Å, periodic boundary conditions were applied, and the interactions were truncated using the minimum image convention.[24]

Three different types of displacements were used in the simulations, viz. (i) translational and rotational displacement of a single particle (protein or polyelectrolyte bead), (ii) pivot rotation of a part of the polyelectrolyte chain, and (iii) translation

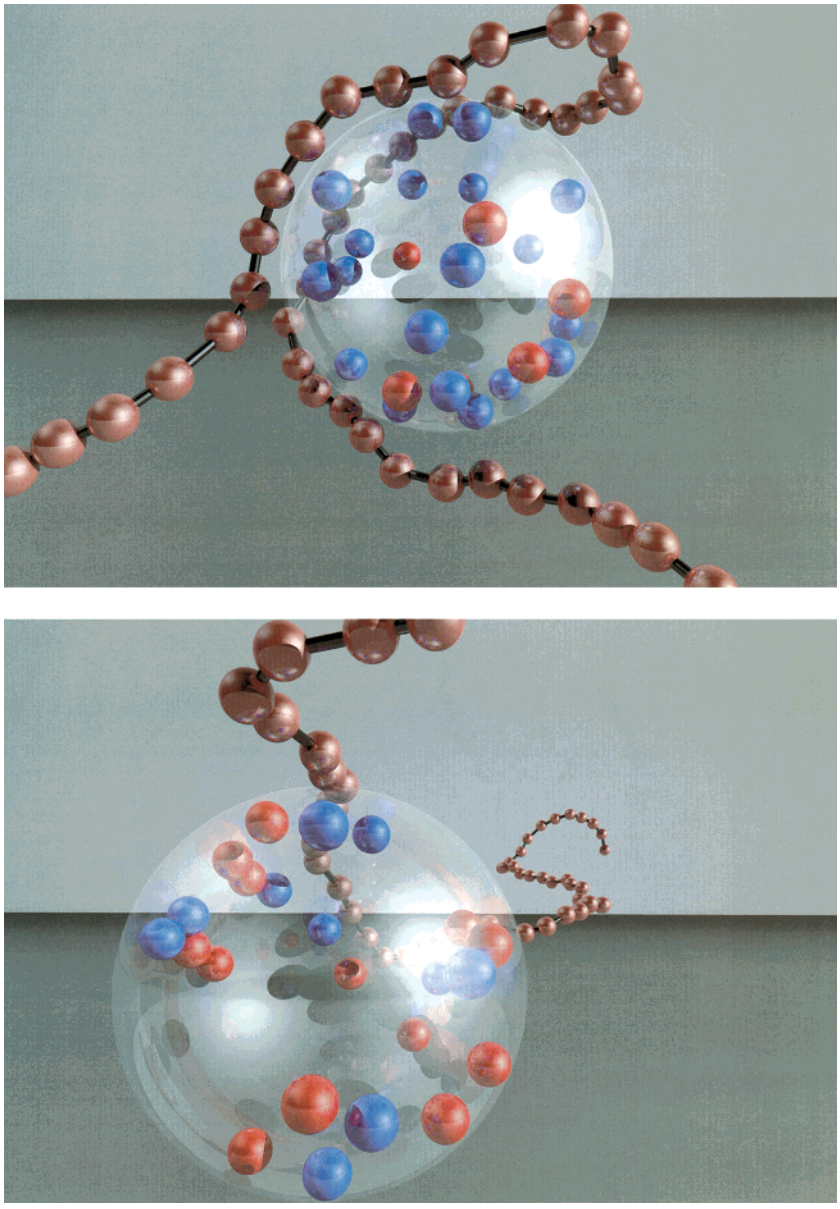

Figure 2. Snapshots from simulations with protein net charge (a) $Z_{prot} = +13$ and (b) -3 at an ionic strength $I = 0.1$ M displaying polyelectrolyte beads (copper colored spheres), positive protein charges (blue spheres), and negative protein charges (red spheres), all with radii 2 Å, and the protein hard sphere (transparent) with radius 18.54 Å.

of the entire polyelectrolyte chain. In step i, a translational displacement in the *x*, *y*, and *z* directions of the polyelectrolyte beads or a translation and a rotation of the protein was performed. The translation length was uniformly sampled in the interval $[-\Delta_i/2,\Delta_i/2]$ and the rotation angle in $[-\theta_i/2,\theta_i/2]$, where Δ_i is the maximum translational parameter and θ_i the maximum rotation parameter for particle of type *i*. A rotation of the protein was effective, since the protein possesses a nonspherical charge distribution. The pivot rotations were only applied to the polyelectrolyte, and the rotation was applied on a randomly selected bond. The rotation angle was uniformly sampled in the interval $[-\alpha/2,\alpha/2]$, where α is the maximum rotation parameter. Translational displacement in the *x*, *y*, and *z* directions of the whole chain was also performed. The translation length was uniformly sampled in the interval $[-\delta/2,\delta/2]$, where δ is the maximum translational parameter. The displacement parameters of the different trial moves were $\Delta_{bead} = 2$ Å, $\Delta_{protein} = 15$ Å, $\theta_{protein} = 360°$, $\alpha = 360°$, and $\delta = 10$ Å, and typical probabilities of the different types of displacements were $P_{part} = 0.85$, $P_{pivot} = 0.10$, and $P_{chain} = 0.05$.

After equilibration, simulations were typical carried out using 10^6 MC passes (attempted trial moves per particle). Reference simulations of the polyelectrolyte only were converged already after 10^5 MC steps. Reported uncertainties were based on a division of the simulations into 10 subbatches.

Results and Discussion

The protein−polyelectrolyte intermolecular structure depends strongly on the pH of the solution through the charge status of the protein. As an initial illustration, Figure 2 displays two snapshots of the model system at pH 3 and 12, respectively, at the ionic strength $I = 0.1$ M. At the lower pH, where the protein net charge is $Z_{prot} = +13$, Figure 2a shows that the negatively charged polyelectrolyte firmly wraps the protein, which we refer to as a strong complexation. On the other hand, at the higher pH, where the net charge is $Z_{prot} = -3$, Figure 2b displays that

the polyelectrolyte has only a limited contact with the protein, which we refer to as a weak complexation. Thus, even at the ionic strength $I = 0.1$ M, corresponding to a Debye screening length of 9.6 Å, the electrostatic interaction between the protein and the polyelectrolyte seems to be important. In the following, we will develop this picture further by first examining the structure of the complex in more detail and later also the properties of the polyelectrolyte.

Protein−Polyelectrolyte Complex. The accumulation of the negatively charged polyelectrolyte beads in the neighborhood of the protein is conveniently represented by the so-called running coordination number (RCN), rcn(r). With the protein center as the origin, rcn(r) denotes the number of polyelectrolyte beads within the distance r from the center. For a random distribution of the polyelectrolyte beads in the system, we would expect $\mathrm{rcn}_{\mathrm{random}}(r) = (N_{\mathrm{bead}}/L^3)(4\pi/3)r^3 = 3.9 \times 10^{-6}\ r^3$ Å^{-3} with, e.g., $\mathrm{rcn}_{\mathrm{random}}(40\ \text{Å}) = 0.3$. Thus, $\mathrm{rcn}(r')/\mathrm{rcn}_{\mathrm{random}}(r') > 1$ implies an accumulation of polyelectrolyte beads within $r < r'$, whereas $\mathrm{rcn}(r')/\mathrm{rcn}_{\mathrm{random}}(r') < 1$ indicates a depletion of the beads in this region.

Figure 3 shows RCN using the center of the protein as the origin at various protein net charges and for the three ionic strengths. A common feature for the displayed RCN's is the increase of the accumulated polyelectrolyte beads as the protein becomes less negatively and more positively charged. Second, the influence of the protein net charge on the polyelectrolyte accumulation generally increases as the ionic strength is reduced.

In more detail, at $I = 0.5$ M Figure 3a shows that even at the highest pH with the most negatively charged protein ($Z_{\mathrm{prot}} = -13$), the net repulsive protein−polyelectrolyte electrostatic interaction is not sufficient to prohibit a complexation. As the protein net charge becomes less negative or more positive, the strength of the protein-complex grows as deduced from the large increase in the number of polyelectrolyte beads in the neighborhood of the protein. When the ionic strength is reduced to $I = 0.1$ M, the influence of Z_{prot} on the complexation increases. Figure 3b shows that the most negatively charged proteins now completely repel the polyelectrolyte. A weak complexation starts to appear first at $Z_{\mathrm{prot}} \approx -6$. We recall that the strength of the short-range attraction was adjusted to give the onset of complexation at $Z_{\mathrm{prot}} \approx -6$ at $I = 0.1$ M. Finally, at $I = 0.05$ M, the trends observed for negatively charged proteins continues. The protein has to be nearly neutral ($Z_{\mathrm{prot}} \approx -3$) before the complexation starts to become substantial. For high Z_{prot} at the lowest ionic strength, the RCN displays a pronounced bend and levels off at high r, whereas at high ionic strength, the change in curvature of the RCN at increasing r is more gradual. This implies that the density of polyelectrolyte beads in the region $r > 25$ Å is lower at $I = 0.05$ M as compared to $I = 0.5$ M. The origin is of course the increased bead−bead repulsion at the lower ionic strength leading to a more stretched tail configuration as illustrated in Figure 2b.

The accumulation of polyelectrolyte beads in the nearest neighborhood of the protein is more clearly demonstrated by considering the number of polyelectrolyte beads near the protein surface $N^{\mathrm{c}}_{\mathrm{bead}}$. Figure 4 shows $N^{\mathrm{c}}_{\mathrm{bead}}$ as a function of the protein net charge at different ionic strengths where beads within 4.9 Å from the protein surface is considered (i.e., $r_{\mathrm{prot-bead}} \le r_{\mathrm{contact}} \equiv R_{\mathrm{prot}} + R_{\mathrm{bead}} + 4.9$ Å). At the two lowest ionic strengths, it is clear that the onset of complexation at increasing Z_{prot} is fairly sharp and appears at $Z_{\mathrm{prot}} \approx -6$ at $I = 0.1$ M and at $Z_{\mathrm{prot}} \approx -3$ at 0.05 M. Moreover, at the largest positive protein charge, $Z_{\mathrm{prot}} = +19$, $N^{\mathrm{c}}_{\mathrm{bead}}$ displays a weak but nontrivial dependency on the ionic strength. At decreasing ionic strength, $N^{\mathrm{c}}_{\mathrm{bead}}$ first increases, whereas at even lower ionic strength, $N^{\mathrm{c}}_{\mathrm{bead}}$ increases again; hence, an optimum of $N^{\mathrm{c}}_{\mathrm{bead}}$ appears in the interval $0.05\ \mathrm{M} < I < 0.5$ M.

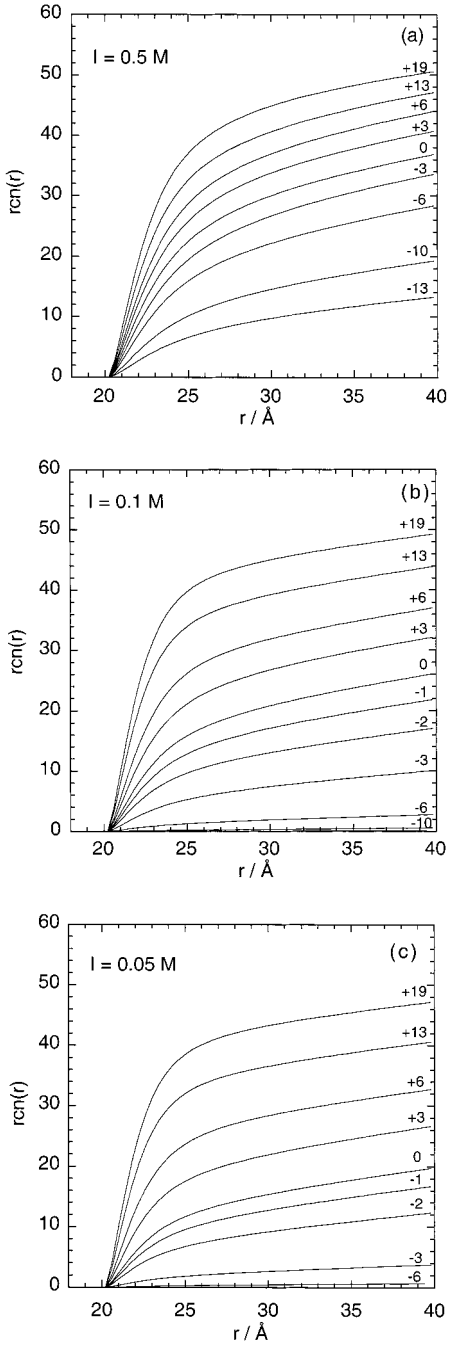

Figure 3. Running coordination number rcn(r) displaying the number of polyelectrolyte beads within the distance r from the protein center at an ionic strength (a) $I = 0.5$, (b) 0.1, and (c) 0.05 M at indicated protein net charge. In panel b with $Z_{\mathrm{prot}} = -13$ and in panel c with $Z_{\mathrm{prot}} = -13$ and -10, the curves cannot be distinguished from the x axis.

Further information on the protein−polyelectrolyte complexation is provided by the probability for contact between the protein and individual polyelectrolyte beads $P^{\mathrm{c}}(i_{\mathrm{bead}})$. The value zero implies that this bead is never in contact with the protein, and the value one that this bead is in contact with the protein during the whole simulation. Here, contact is defined as above, i.e., $r_{\mathrm{prot-bead}} \le r_{\mathrm{contact}}$, but using a 5.0 Å layer. Such an analysis was previously used to analyze the complexation between a polyelectrolyte and oppositely charged macroions in solution.[25]

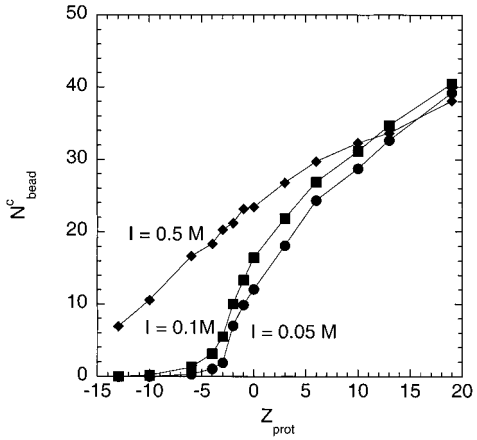

Figure 4. Number of polyelectrolyte beads within 4.9 Å from the protein surface N^c_{bead} as a function of the protein net charge Z_{prot} at indicated ionic strength.

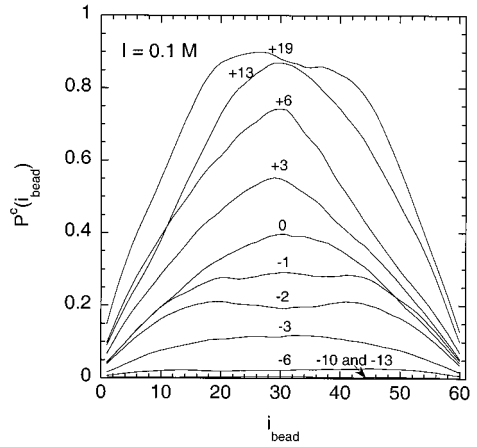

Figure 5. Probability of contact between the protein and different polyelectrolyte beads $P^c(i_{bead})$ as a function of the bead number i_{bead} at an ionic strength $I = 0.1$ M at indicated protein net charge.

Figure 5 displays these complexation probabilities as a function of the bead number at various protein net charges at $I = 0.1$ M. The probability functions are all reasonably symmetric with respect to reflection at bead 30, i.e., the middle of the polymer chain. This indicates that the mobility in the configurational space is sufficient for an adequate sampling of the complexation between the protein and the different beads of the polyelectrolyte. We find that the largest probability to participate in a complex formation is found for the central beads. The complexation probability for these beads to be complexed amounts to ca. 0.8−0.9 for the most positively charged protein. The probability reduces for beads being closer to the chain ends, and considerable dangling tails are observed as illustrated in Figure 2a. As the protein net charge becomes less positive, the complexation probabilities gradually decrease.

Thus, at the highest ionic strength, i.e., $I = 0.5$ M, it is obvious that short-range interaction represented by the $1/r^6$ potential is important for the protein−polyelectrolyte complexation. As the electrostatic forces become less screened at lower ionic strength, the probability of contact with the negatively charged polymer decreases for negatively or slightly positively charged proteins. For negatively charged proteins, clearly at low ionic strength, the attractive short-range $1/r^6$ potential becomes less important in relation to the repulsive electrostatic protein−polyelectrolyte interaction. For the most positively charged proteins, the adsorbed amount first increases and then decreases as the ionic strength is reduced. The initial increase is attributed to the fact that the protein−polyelectrolyte attraction dominates over the intramolecular polyelectrolyte repulsion between the polyelectrolyte beads. However, as the ionic strength is reduced, the intramolecular electrostatic repulsion becoming relatively more important, owing to more separated polyelectrolyte beads starting to repel each other. Obviously, the location of the maximum depends on Z_{prot}, and an increase of Z_{prot} would shift the location of the maximum to lower ionic strength.

As mentioned above, previous experimental studies[10,11] of lysozyme−polymer complexation at the ionic strength of 0.1 M have shown that there is an onset of complexation already when the polymer and protein have the same charge. By judging from the RCN (Figures 3b and 4), it is reasonable to assign an onset of a complexation at a protein net charge of $Z_{prot} \approx -6$ at $I = 0.1$ M. Of course a precise identification of the onset is not possible, since the extent of complexation defined by the RCN gradually increases with a reduced negative or an increased positive protein net charge. Nevertheless, given our adjustment of the strength of the short-range attraction, the model predicts that at the ionic strength $I = 0.5$ M a complexation appears already at a protein net charge −13.

2D Polymer Distribution. Although the protein net charge is clearly of importance in determining the complexation, it is interesting to consider the effects of the protein charge distribution on the complex formed. To obtain an overview of how the polymer is distributed over the protein surface, the polymer density in a 4 Å thick slice through the protein was calculated. The histograms were based on a cylindrical geometry defined by radius r, height z, and angle φ using a protein-based coordinate system. A polymer bead was regarded as inside the plate and thus counted if $|z| \leq 2$ Å.

Figure 6 shows such two-dimensional distribution functions for $Z_{prot} = +6$ and -6 at $I = 0.05$ M. It is clearly visible that some regions near the positive charges have much higher polymer density than others. This is valid for both positive and negative protein net charges even though the level is much lower for the negative net charge. Obviously, the polymer binds to the protein in a patchwise manner with the negatively charged polyelectrolyte beads preferentially located close to the positive protein charges. This effect was found at all ionic strengths investigated, although the quantitative effect decreases with an increasing ionic strength.

The distribution of the polyelectrolyte beads around the protein charges was quantified by calculating running coordination number of the polyelectrolyte beads with positive or negative protein charges as those of the origin. Figure 7 shows that the negative polyelectrolyte beads indeed are closer to the positive protein charges than to the negative ones. At the protein net charge $Z_{prot} = +6$, there is on the average 1.2 polyelectrolyte beads within 9 Å from the center of a positive charge but only 0.4 within the same distance from a negative one. At the protein net charge $Z_{prot} = 0$, the corresponding numbers are 0.7 and 0.2, respectively. Thus, at short separation, there is typically three times more polyelectrolyte beads near a positive protein charged as compared to a negative one. However, at bead−protein charge distances comparable to the protein size, the RCN curves for the positive and negative protein charges naturally approach each other.

Polyelectrolyte Properties. Various properties of the polyelectrolyte chain characterizing its extension and shape have also been calculated for the different protein net charges and ionic strengths as well as for the protein-free systems. We will here examine (i) the average angle between three consecutive

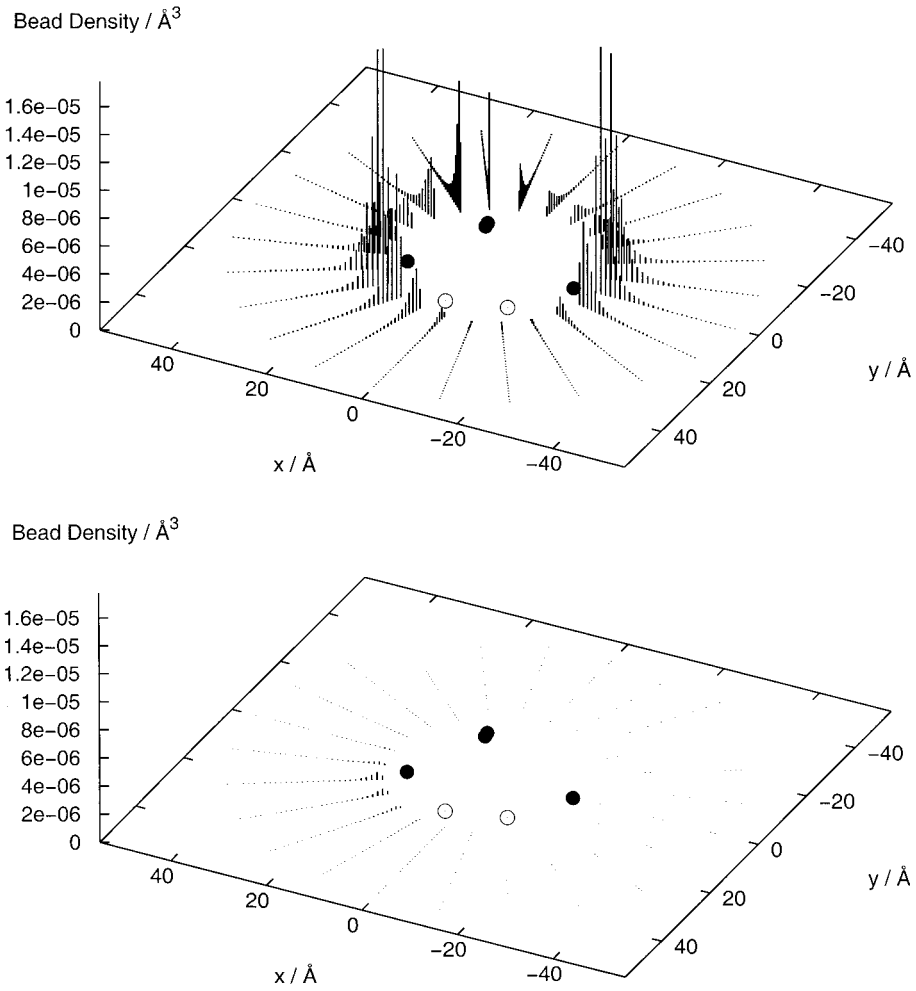

Figure 6. Polymer density in a 4 Å thick slice through the center of the protein with protein net charge (a) $Z_{prot} = +6$ and (b) -6 at the ionic strength $I = 0.05$ M. The charges shown are those in a 14 Å thick slice projected on the plane $z = 0$. The z coordinates of the positive protein charges (filled circles) are -1.02, 2.95, 6.93, and -1.02 Å and of the negative protein charges (open circles) -6.56 and -5.11 Å.

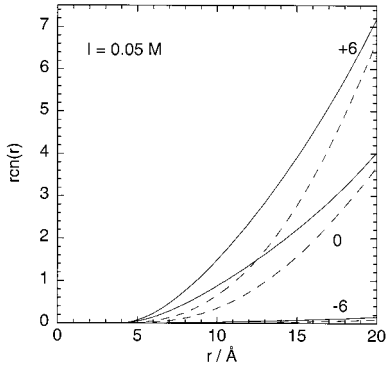

Figure 7. Running coordination number rcn(r) displaying the number of polyelectrolyte beads within the distance r from the positive protein charges (solid curves) and the negative protein charges (dashed curves) at the ionic strength $I = 0.05$ M and at indicated protein net charge.

beads ($\langle\alpha\rangle$), where α is defined as in the Model section, (ii) the root-mean-square (rms) end-to-end distance ($\langle R_{ee}^2\rangle^{1/2}$), and (iii) the shape ratio $\langle R_{ee}^2\rangle/\langle R_G^2\rangle$, where $\langle R_G^2\rangle^{1/2}$ is the rms radius of gyration. For a Gaussian chain, the shape ratio is 6, whereas it is 12 in the limit of a rigid rod.

In the absence of the protein, Figure 8a (open symbols) shows that the average angle between three consecutive beads increases as the ionic strength decreases. Hence, increasing electrostatic repulsion appearing at lowering ionic strength leads to a locally more stretched chain. In the presence of the protein, $\langle\alpha\rangle$ is unaffected until Z_{prot} becomes sufficiently high. The critical Z_{prot} at which $\langle\alpha\rangle$ starts to reduce is below -13 at $I = 0.5$ M, ca. -5 at 0.1 M, and ca. -3 at 0.05 M. At high Z_{prot}, $\langle\alpha\rangle$ is less dependent on the ionic strength as compared to the dependence on I at low Z_{prot} or in a protein-free system. In Figure 8b, the rms end-to-end distance $\langle R_{ee}^2\rangle^{1/2}$ is given. For the protein-free system, $\langle R_{ee}^2\rangle^{1/2}$ increases, i.e., the chain becomes more expanded, as the ionic strength is lowered. In the presence of the protein, $\langle R_{ee}^2\rangle^{1/2}$ depends on Z_{prot} in way similar to that of $\langle\alpha\rangle$. Finally, Figure 8c shows the shape ratio $\langle R_{ee}^2\rangle/\langle R_G^2\rangle$. Not unexpectedly, in the protein-free system, the polyelectrolyte becomes more elongated as the ionic strength is reduced. In the presence of the protein, the shape ratio is unaffected until again Z_{prot} becomes sufficiently large to create a complex and where the complexation causes the polymer to adapt a more condensed conformation. At large positive net charge, the precision of $\langle R_{ee}^2\rangle/\langle R_G^2\rangle$ is impaired substantially, probably due to the slower mobility of the polyelectrolyte chain in the configurational space caused by the strong complex formed.

To summarize, at sufficiently negative protein net charge, the local stretching, the size, and the shape of the polyelectrolyte are unaffected by the presence of the protein. However, $\langle\alpha\rangle$, $\langle R_{ee}^2\rangle^{1/2}$, and $\langle R_{ee}^2\rangle/\langle R_G^2\rangle$, all start to change at values of Z_{prot} where we previously concluded that the complexation starts to appear. Hence, at the onset of complexation, the polyelectrolyte becomes (on average) locally less stretched, and its overall

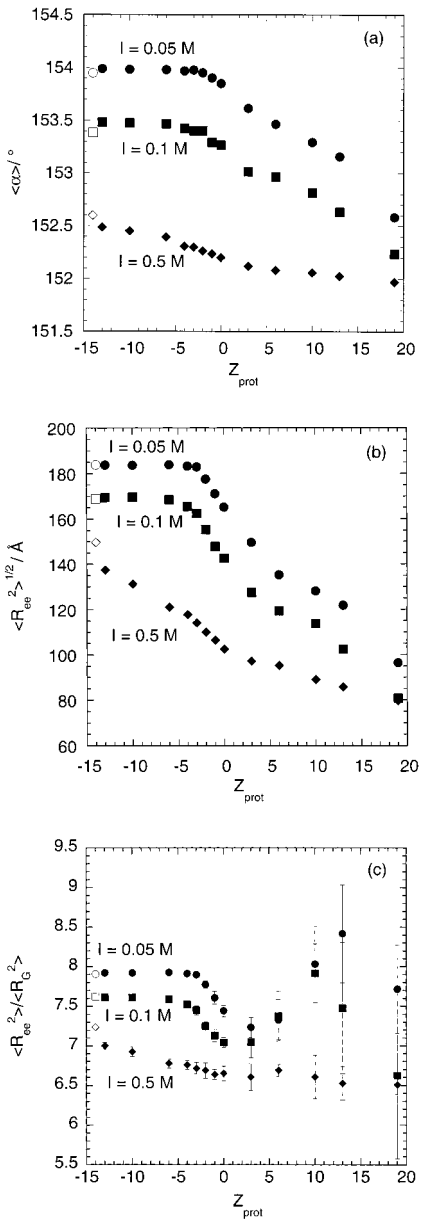

Figure 8. (a) Average angle between three consecutive polymer beads $\langle\alpha\rangle$, (b) root-mean-square end-to-end distance $\langle R_{ee}^2\rangle^{1/2}$, and (c) shape ratio $\langle R_{ee}^2\rangle/\langle R_G^2\rangle$ as a function of the protein net charge Z_{prot} at ionic strengths $I = 0.05$ M (filled circles), 0.1 M (filled squares), and 0.5 M (filled diamonds). The corresponding properties for protein-free systems are given by open symbols. The uncertainties are ±3 standard deviations and often smaller than the symbols.

extension is reduced. The shape, as monitored by the shape ratio $\langle R_{ee}^2\rangle/\langle R_G^2\rangle$, becomes more Gaussian-like. As the complexation becomes stronger, either by a more positively charged protein or a lower ionic strength, the magnitude of these changes increases.

A contraction of the polyelectrolyte upon complexation has been found earlier from simulations of uniformly charged spheres and their complexation with polyelectrolytes.[25] The collapse of polymer chains in the presence of small colloidal spheres has also been examined theoretically, and the conclusion was drawn that chain collapse occurs when the mutually excluded volumes of the segments, renormalized by the concentration fluctuations of the colloids, become negative.[26] Overall, our present result on the polymer conformation are in qualitative agreement with these previous findings.

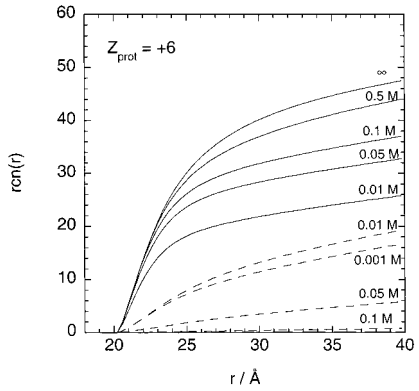

Figure 9. Running coordination number rcn(r) displaying the number of polyelectrolyte beads within the distance r from the protein center with a protein net charge $Z_{prot} = +6$ with (solid curves) and without (dashed curves) the attractive short-range $1/r^6$ potential at indicated ionic strength.

Electrostatic Protein−Polyelectrolyte Interaction Only. To further examine the interplay between the electrostatic and the short-range attractive interactions, simulations without the short-range interaction were performed. Figure 9 shows RCN for $Z_{prot} = +6$ at different ionic strengths with (solid curves) and without (dashed curves) the $1/r^6$ potential. Generally, for this protein net charge, the complexation becomes much weaker in the absence of the attractive short-ranged potential. Moreover, as a consequence of this weaker complexation, the system without the $1/r^6$ potential explores the configurational space more efficiently.

Again, we focus on the values of the RCN at $r = r_{contact}$. In the absence of the short-range potential, a complex starts to appear at $I \approx 0.05$ M, increasing as the ionic strength is reduced and approaching a maximum at $I \approx 0.01$ M. Obviously, the complexation is here driven by electrostatic interactions only, which becomes more important as the ionic strength is reduced. The maximum appears when the intrachain repulsion becomes comparable to the protein−polyelectrolyte attraction, and at an even lower ionic strength ($I = 0.001$ M), the polyelectrolyte becomes more stretched, as demonstrated by the reduced RCN at large distances (see Figure 9). When the short-range potential is included, Figure 9 shows that the complexation becomes weaker as the ionic strength is reduced as discussed above. Here, results for $I = 0.01$ M and $I \rightarrow \infty$ are also included.

An experimental observation of a similar dependence of the strength of the protein−polymer complex on the ionic strength has been made. Hattori et al.[27] found that the binding of negatively charged β-lactoglobulin to negatively charged sodium poly(styrenesulfonate) at pH 7 displayed a maximal binding constant at intermediate ionic strength.

The accumulation of polyelectrolyte beads near the protein at various protein net charges is shown in Figure 10. At $I = 0.1$ M, it is again demonstrated that a complexation in the absence of the attractive short-range interaction requires a positively net charged protein. This should be compared with Figure 4 where the complexation with the short-range attraction present starts already at $Z_{prot} \approx -6$. Figure 10 also shows that the onset of the complexation is driven toward less positively charged proteins as the ionic strength is reduced and appears close to $Z_{prot} = 0$ at low ionic strength.

Thus, for $Z_{prot} = +6$ and with the particular strength of the short-range attraction selected, the short-range attraction plays not only the dominant role for the adsorption at high ionic strength, but also an important role at $I = 0.01$ M. This prominent role of the short-range attraction found is in agree-

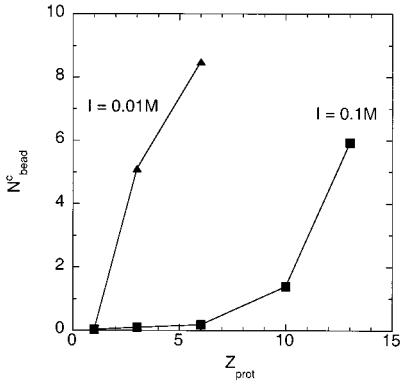

Figure 10. Number of polyelectrolyte beads within 4.9 Å from the protein surface N^c_{bead} as a function of the protein net charge Z_{prot} without the attractive short-range $1/r^6$ potential at indicated ionic strength.

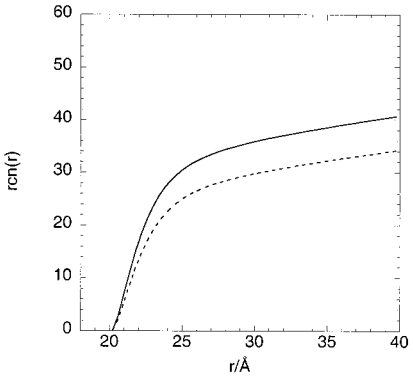

Figure 11. Running coordination number rcn(r) displaying the number of polyelectrolyte beads within the distance r from the protein center with a protein net charge $Z_{prot} = +10$ at the ionic strength $I = 0.1$ M with the discrete charge model (solid curve) and the simplified monopole model (dashed curves).

ment with the experimental findings of complexes observed for PVS at net charges as low as $Z_{prot} = -7$.[10,11]

The complexation between a polyelectrolyte and an oppositely charged patterned surface[18] as well as between polyelectrolytes and oppositely charged spheres and planar surfaces[19] involving only electrostatic interactions has previously been studied by MC simulations. Moreover, Ellis et al.[20] have investigated the adsorption of a polyelectrolyte to a charged surface with a random distribution of positive and negative charges and with different net charges using screened Coulomb interactions. They observed that a polyelectrolyte could adsorb to a surface with randomly distributed positive and negative charges, even if the net charge of the surface was of the same sign as that of the polyelectrolyte. The region to which the polyelectrolyte was adsorbed was found to be more attractive than the surface as a whole. This is in analogy with our findings displayed in Figure 7, which showed that the negative polyelectrolyte beads are on the average closer to the positive protein charges as compared to the negative ones. However, in the present investigation, without short-range attraction, we did not observe an adsorption to the spherically charged surface unless the protein carries a net charge of opposite sign to the polyelectrolyte.

Effects of the Discrete Charges. To further investigate the role of the discrete charge distribution, simulations were made also for a system with the net charge placed at the center of the protein corresponding to a homogeneous surfaced charge density. The RCN's for the two charge models at $Z_{prot} = +10$, where the discrete protein charge model possesses 19 positive charges and 9 negative ones, have been examined. Figure 11 shows that the homogeneous surface charge model gives a lower amount of complexed polyelectrolyte beads. Moreover, a more elongated chain conformation with slightly larger average angle between three consecutive beads and slightly larger root-mean-square end-to-end distance were found, which primarily is attributed to the weaker complex formation. It is reasonable to attribute the additional spatial correlations between the polyelectrolyte beads and the protein charges to the enhanced polyelectrolyte adsorption in the discrete charge model. Thus, a protein model with discrete charges may lead to a stronger complexation as well as to an inhomogeneous polyelectrolyte bead distribution as compared to a homogeneous surface charge distribution. The complexation is driven by enthalpy, and the discrete charge distribution gives an increased gain in enthalpy upon complexation as compared to the case of homogeneous charge distribution. Finally, the appearance of some ambiguity on how the hard-sphere volumes affect the electrostatic screening hampers a more definite comparison between the two charge models. This ambiguity is lifted first when the small ions enter the model explicitly.

Summary

The properties of a system representing an aqueous system of one lysozyme molecule and one polymer were investigated using Monte Carlo simulations. Electrostatic interactions were found to play an important role for the complex formation in this system, particularly at high protein net charge and when the electrostatic interactions are not extensively screened by large excess of electrolyte concentrations. It was also demonstrated that electrostatic interactions are not the only driving force behind the complexation in the system. To obtain results comparable to experimental ones, an attractive short-range potential between the protein and the polyelectrolyte beads was needed, and the role of this attraction was examined. Upon complexation, the polyelectrolyte contracts, and the distribution of the polyelectrolyte beads became laterally inhomogeneous due to the electrostatic forces. Finally, we also demonstrated that a protein model with a homogeneous surface charge density gave rise to a lower amount of complexed polyelectrolyte beads, owing to lacking spatial charge−charge correlations.

Acknowledgment. Dr. Bengt Jönsson and Anna Stenstam, Lund University, and Prof. Thomas Arnebrant, Institute for Surface Chemistry (YKI), are gratefully acknowledged for helpful discussions. Financial support from the Swedish Foundation for Strategic Research (SSF) through the graduate school Colloid and Interface Technology (CIT) and from the Swedish National Research Council (NFR) is gratefully acknowledged.

References and Notes

(1) Tolstoguzov, V. B. *Food Hydrocolloids* **1991**, *4*, 429−468.

(2) Ahmed, L. S.; Xia, J.; Dubin, P. L. *J. M. S. Pure Appl. Chem.* **1994**, *A31*, 17−29.

(3) Dubin, P. L.; Gao, J.; Mattison, K. *Separation Purification Methods* **1994**, *23*, 1−16.

(4) Xia, J.; Dubin, P. L. Protein-Polyelectrolyte Complexes. In *Macromolecular Complexes in Chemistry and Biology*; Dubin, Bock, Davis, Schulz, Thies, Eds.; Springer-Verlag: Berlin, 1994; pp 247−271.

(5) Kokufuta, E. Complexation of Proteins with Polyelectrolytes in a Salt-Free System and Biochemical Characteristics of the Resulting Complexes. In *Macromolecular Complexes in Chemistry and Biology*; Dubin, Bock, Davis, Schulz, Thies, Eds.; Springer-Verlag: Berlin, 1994; pp 301−325.

(6) Schmitt, C.; Sanchez, C.; Desobry-Banon, S.; Hardy, J. *Crit. Rev. Food Sci. Nutrition* **1998**, *38*, 689−753.

(7) Hunter, A. *Hoppe-Seyler's Z. Phys. Chem.* **1907**, *53*, 526−538.

(8) Jong, H. G. B. d. Complex Colloid Systems. In *Colloid Science*; Kruyt, H. R., Ed.; Elsevier: Amsterdam, 1949; Vol. II, pp 335−432.
(9) Kossel, A. *Protamines and Histones*; Longmans & Co: London, 1928.
(10) Park, J. M.; Muhoberac, B. B.; Dubin, P. L.; Xia, J. *Macromolecules* **1992**, *25*, 290−295.
(11) Xia, J.; Dubin, P. L.; Kim, Y.; Muhoberac, B. B.; Klimkowski, V. J. *J. Phys. Chem.* **1993**, *97*, 4528−4534.
(12) Mattison, K. W.; Brittain, I. J.; Dubin, P. L. *Biotechnol. Prog.* **1995**, *11*, 632−637.
(13) Kopaciewicz, W.; Rounds, M. A.; Fausnaugh, J.; Regnier, F. E. *J. Chromatogr.* **1983**, *266*, 2−21.
(14) Joanny, J.-F. *J. Phys. II* **1994**, *4*, 1281−1288.
(15) Odijk, T. *Macromolecules* **1990**, *23*, 1875−1876.
(16) Goeler, F. v.; Muthukumar, M. *J. Chem. Phys.* **1994**, *100*, 7796−7803.
(17) Muthukumar, M. *J. Chem. Phys.* **1987**, *86*, 7230−7235.
(18) Muthukumar, M. *J. Chem. Phys.* **1995**, *103*, 4723−4731.
(19) Kong, C. Y.; Muthukumar, M. *J. Chem. Phys.* **1998**, *109*, 1522−1527.
(20) Ellis, M.; Kong, C. Y.; Muthukumar, M. *J. Chem. Phys.* **2000**, *112*, 8723−8729.
(21) Ramanadham, M.; Sieker, L. C.; Jensen, L. H. *Acta Crystallogr., Sect. B* **1990**, *46*, 63−69.
(22) Blake, C. C. F.; Koenig, D. F.; Mair, G. A.; North, A. C. T.; Phillips, D. C.; Sarma, V. R. *Nature* **1965**, *206*, 757−761.
(23) Coffman, J. L.; Lightfoot, E. N.; Root, T. W. *J. Phys. Chem. B* **1997**, *101*, 2218−2223.
(24) Allen, M. P.; Tildesley, D. J. *Computer Simulation of Liquids*; Oxford University Press: Oxford, 1987.
(25) Jonsson, M.; Linse, P. *J. Chem. Phys.* **2001**, *115*, 3406−3418.
(26) Schoot, P. v. d. *Macromolecules* **1998**, *31*, 4635−4638.
(27) Hattori, T.; Hallberg, R.; Dubin, P. L. *Langmuir* **2000**, *16*, 9738−9743.
(28) Kuramitsu, S.; Hamaguchi, K. *J. Biochem.* **1980**, *19*, 1215−1219.